Journal of Innovative Optical Health Sciences
Vol. 2, No. 2 (2009) 189–200

World Scientific
www.worldscientific.com

DETECTION OF Ca^{2+}-DEPENDENT NEURONAL ACTIVITY SIMULTANEOUSLY WITH DYNAMIC CHANGES IN CEREBRAL BLOOD VOLUME AND TISSUE OXYGENATION FROM THE LIVE RAT BRAIN

CONGWU DU[*,‡,‖], ZHONGCHI LUO[†], MEI YU[*], HELENE BENVENISTE[*,‡], MELISSA TULLY[†], RUBING PAN[§] and BRITTON CHANCE[¶]

[*]*Medical Department, Brookhaven National Laboratory*
Upton, NY 11973-5000, USA

[†]*Department of Biomedical Engineering, SUNY at Stony Brook*
Stony Brook, NY 11794, USA

[‡]*Department of Anesthesiology, SUNY at Stony Brook*
Stony Brook, NY 11794, USA

[§]*Department of Biology, University of Illinois at Urbana-Champaign*
Urbana, IL 61801

[¶]*Department of Biophysics and Physical Chemistry*
University of Pennsylvania, Philadelphia, PA, 19104
[‖]*congwu@bnl.gov*

We present a catheter-based optical diffusion and fluorescence (ODF) probe to study the functional changes of the brain *in vivo*. This ODF probe enables the simultaneous detection of the multi-wavelength absorbance and fluorescence emission from the living rat brain. Our previous studies, including a transient stroke experiment of the rat brain as well as the brain response to cocaine, have established the feasibility of simultaneously determining changes in cerebral blood volume (CBV), tissue oxygenation (S_tO_2) and intracellular calcium ($[Ca^{2+}]_i$, using the fluorescence indicator $Rhod_2$). Here, we present our preliminary results of somatosensory response to electrical forepaw stimulation obtained from the rat cortical brain by using the ODF probe, which indicate that the probe could track brain activation by directly detecting $[Ca^{2+}]_i$ along with separately distinguishing CBV and S_tO_2 in real time. The changes of CBV, S_tO_2 and $[Ca^{2+}]_i$ are comparable with the blood-oxygen-level-dependent (BOLD) response to the stimulation obtained using functional magnetic resonance imaging (fMRI). However, the high temporal resolution of the optical methodology is advanced, thus providing a new modality for brain functional studies to understand the hemodynamic changes that underlie the neuronal activity.

Keywords: Optical spectroscopy; calcium fluorescence; $Rhod_2$ labeling; brain ischemia and cocaine addiction; forepaw stimulation.

1. Introduction

The measurement of local changes in brain hemodynamics and oxygenation induced by cognitive tasks is widely used to advance our understanding of the neural bases of perception, attention, memory, language, and a drug-induced addiction process.[1,2] For example, functional magnetic resonance imaging (fMRI) and positron emission tomography (PET) record local fluctuations in cerebral hemodynamics associated with neural activation[3–5] while electroencephalography (EEG) and magnetoencephalography (MEG) measure current flows directly induced by synaptic activity. fMRI has high spatial resolution whereas EEG and MEG have high temporal resolution.[6] Compared to fMRI, optical technology can directly access the changes in oxygenated and deoxygenated hemoglobin, as well as can quantitatively determine the hemoglobin concentration and its oxidative state with a higher temporal resolution.[7,8] Therefore, it has also been used in brain functional studies. Additionally, optical detection in combination with fluorescent techniques enables us to track intracellular calcium ($[Ca^{2+}]_i$) changes which are directly associated with neuronal activity. Thus, optical techniques have a great potential for the brain functional studies because they permit tracking of neural activation directly by measuring cellular response (i.e., $[Ca^{2+}]_i$ changes) along with separately distinguishing vasodynamic changes (e.g., cerebral blood flow, blood volume and tissue oxygenation) following brain activation.

We have developed a catheter-based optical diffusion fluorescence (ODF) probe to detect the changes of cerebral blood volume (CBV) and tissue oxygenation (S_tO_2) along with fluorescent-dependent $[Ca^{2+}]_i$ transients directly from the live rat cortex.[9] Recently, we validated this technique by using animal models to characterize *in vivo* cerebral hemodynamics and $[Ca^{2+}]_i$ changes in the cortical brain in response to physiological insult or pharmacological challenge.[9,10] Here, we briefly review the technical aspects of our ODF probe, and summarize its preclinical applications. The results demonstrate that the ODF probe has a great sensitivity to track multi-parameters, such as CBV, S_tO_2 and $[Ca^{2+}]_i$ from the living brains, which permit us to study not only the cortical vascular dynamics but also direct neuronal responses to physiological or pharmacological challenge in normal or diseased brains.

2. Materials and Method

2.1. *Prototype catheter-based ODF probe*

Figure 1(a) shows a systemic diagram of the multi-wavelength ODF probe designed to detect the changes of the local CBV, S_tO_2 and $[Ca^{2+}]_i$ from the surface of the brain. The system has been described previously.[9] Briefly, it consisted of a 150-W Xenon lamp, a monochromater (Mono-Ex), and the photon detectors for fluorescence (PMT-F) and diffuse reflectance (PMT-A). The lamp was connected to a computer-controlled monochromater to select the incident wavelengths of 548 nm, 555 nm, and 572 nm by time-sharing to sequentially deliver the light at these wavelengths onto the brain surface through one arm of a Y-shape bifurcated fiber-optic bundle. The calcium-dependent fluorescence and diffusive reflectance from the brain tissue were collected by the fiber tip of the common leg and detected by the photon detectors of PMT-F and PMT-A accordingly. The changes in CBV and S_tO_2 could be separately distinguished from the reflectance measured by summing and subtracting the optical densities of the signals at 555 nm and 572 nm (i.e., symmetric wavelengths to the hemoglobin isobestic point). The signals are digitized and stored in a personal computer for data processing. The ratio of Ca^{2+} fluorescence emission at 589 nm over re-emitted excitation reflectance at 548 nm represents the calcium-dependent fluorescence with a minimum influence of physiological interference.

2.2. *Phantom studies to simulate $Rhod_2$ delivery within biological tissue*

Unlike hemoglobin, intracellular calcium cannot be accessed without fluorescence labeling. We used one of the calcium-fluorescent indicators, $Rhod_2$(AM) (Molecular Probes, Eugene, OR, USA) to label the $[Ca^{2+}]_i$ within the brain because it has several advantages over other fluorescence dyes, including (1) the relatively long excitation and emission wavelengths that reduce the attenuation of the light by the tissue absorbers (e.g., hemoglobin, etc.); (2) the reduced contribution of autofluorescence (e.g., NAHD); and (3) the brighter fluorescence while binding-upon calcium ($\sim$100 folds increase). These features allow the $Rhod_2$ to penetrate more

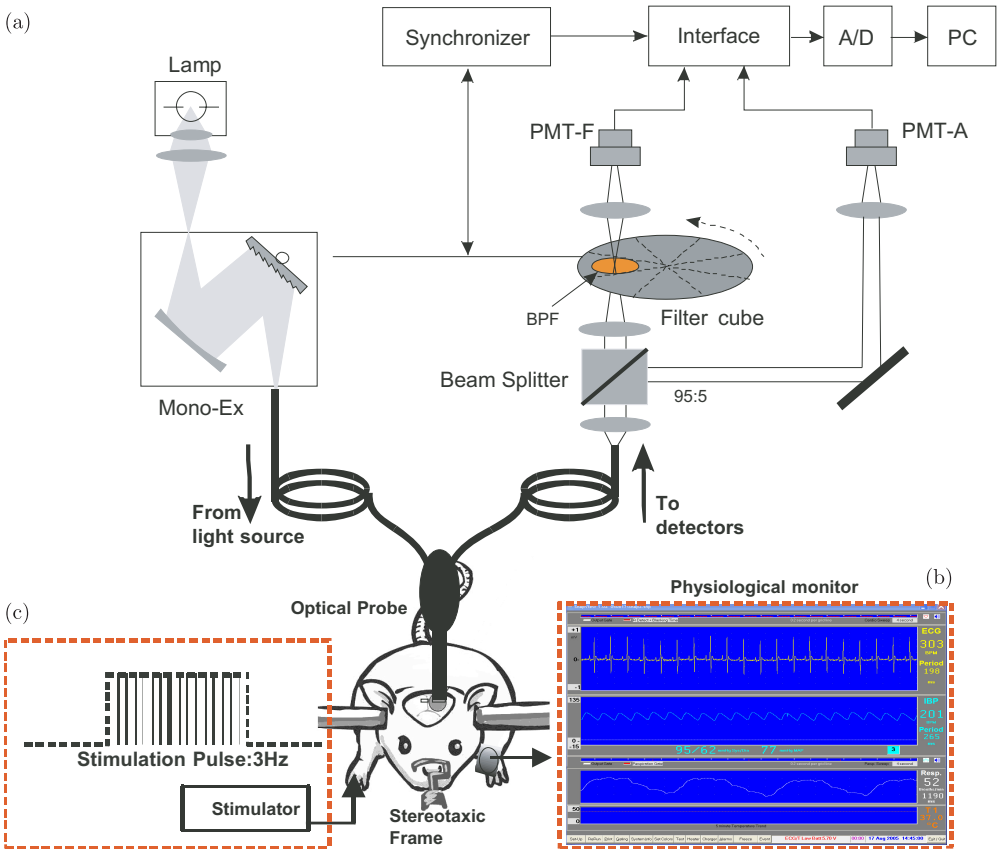

Fig. 1. (a) Diagram of ODF probe used for detecting the changes in CBV, S_tO_2 and $[Ca^{2+}]_i$ fluorescence from the cortical brain of the rat. (b) An example of a real-time physiological monitor during the *in vivo* experiments. (c) Paradigm of electrical stimulation of forepaw to induce a somatosensory response of the rat brain.

deeply into the tissue than other dyes,[11,12] thus ensuring *in vivo* fluorescence measurement with a better signal-to-noise ratio.

To simulate delivery of $Rhod_2$ into the brain and experimentally evaluate $Rhod_2$ distribution within a scattering medium, we have performed phantom studies. The tissue phantom was made of 1% agarose gels mixed with 0.5% intralipid in 7.5 ml PBS (pH = 7.0) to simulate the biological tissue with scatter particles and also eliminate the action of convective flow. The solution of 10-μM $Rhod_2$ (cell impermeable form, Molecular Probes) mixed with 1000-nM Ca^{2+} was used to produce $Rhod_2$-Ca^{2+} fluorescence emission during this phantom study. The solution was microinjected into the phantom which was maintained at a constant temperature of 37°C. Injection rates of 0.1 μl/min, 1 μl/min, and 10 μl/min were conducted during the experiments. Both vertical and oblique injection methods were performed to evaluate the homogeneity of the $Rhod_2$ distribution within the phantom. The diffusion distance of $Rhod_2$ along X, $-X$, Y and $-Y$ directions was evaluated by measuring $Rhod_2$-Ca^{2+} fluorescence emission using a fluorescence microscope (Nikon Eclipse 800).

2.3. *Ex vivo, in vivo animal studies and experimental procedures*

For animal studies, all experimental procedures were approved by the Brookhaven National Laboratory IACUC. The different animal studies were performed and the details of experimental procedures are described as follows.

2.3.1. *General animal preparation*

Experiments were performed on female Sprague–Dawley rats, weighing 300–350 g. Animals were firstly anesthetized with 3% isoflurane, intubated and mechanically ventilated using 100% oxygen gas flow. Anesthesia was maintained with 1.5–2% isoflurane in an O_2/air mixture during the surgery. The right femoral artery and vein were cannulated for continuous blood pressure monitoring, blood gas sampling, and intravenous drug administration

(e.g., α-chloralose). After the surgery, the rat was placed in a stereotaxic frame (Kopf, Frame No. 9) and a small craniotomy was made above the somatosensory cortex of the left side of the brain. For the forepaw stimulation experiment, the isoflurane was discontinued after the surgery, and anesthesia was switched to α-chloralose (initial dose of 50 mg/kg and followed by a continuous infusion of 25 mg/kg/h through femoral vein during the rest of experiment). During the experimental period, the physiological parameters, including the heart rate, blood pressure, and respiration rate and body temperature were monitored in real time (Fig. 1(b)). The body temperature was maintained at about 36.8°C–37.5°C using a heating pad, and $PaCO_2$ level was maintained in the range of 30–45 mmHg by regulating the tidal volume.

2.3.2. *Rhod$_2$(AM) loading into the in vivo brain*

In all of the experiments, the cortical areas of the animal brain were labeled *in vivo* using the fluorescence calcium indicator Rhod$_2$(AM). Initially, 50 μg of Rhod$_2$(AM) (Molecular Probes, Eugene, OR, USA) was dissolved first in 2 μl of dimethysulfoxide (DMSO) and then in 440 μl of distilled water at room temperature. A 30-G needle attached to a stereotaxic micromanipulator was inserted into the cortex ($\sim$1.2–1.5 mm below the surface) with a certain angle ($\sim$30–45°). The Rhod$_2$ solution of 100 μl was infused into the brain at a perfusion flow rate of 3 μl/min using a microinjection pump (CMA/100, Carnegie Medicine, Stockholm, Sweden). This was followed by 60–80 min of waiting time for Rhod$_2$ to be hydrolyzed by intracellular esterases to become membrane-impermeable calcium-binding indicators.

2.3.3. *Monitoring of Rhod$_2$ distribution and its loading effect on the brain*

In order to estimate the distribution of Rhod$_2$ and a possible damage within the brain due to Rhod$_2$ loading, we performed both *ex vivo* experiment of fluorescence images of frozen brains and MRI experiment in living brains. Two types of *ex vivo* fluorescence images were taken with the different imaging scales: one was the cryostatic section image and the other was freeze-trapped redox scanning. For the cryostatic section images, the rat brains ($n = 3$) were quickly removed following the Rhod$_2$ loading, and dipped into a glass container with isopentane cooled with liquid N_2. The frozen brains were then sectioned into horizontal planes at 20-μm thickness (OTF 5000, Jencons), fixed and the fluorescence images were taken using an Epi-fluorescence microscope (Nikon/Eclipse/E800, $\lambda_{ex} = 540$ nm and $\lambda_{em} = 590$ nm). The experiment of freeze-trapped redox scanning was conducted by using a home-built redox scanner at Dr Chance's Laboratory, the technical aspects of which have been extensively reviewed previously.[13] The trapped redox scanner allows measurement of Rhod$_2$-dependent calcium fluorescence simultaneously with NADH and flavoproteins F_p to present the metabolic state of the frozen brain. For MRI experiments, a series of diffusion-weighted MR images were acquired with different b values for the living rat brain 1.5–2 h following the Rhod$_2$ microinjection. The apparent diffusion coefficient (ADC) value was determined accordingly for both the vehicle side and the Rhod$_2$ injection side to evaluate whether there is tissue ischemia/damage due to the Rhod$_2$ loading. The details of MRI acquisition procedure will be described in the following section.

2.3.4. *Cerebral responses to the forepaw stimulation of the rat*

Electrical stimulation of the rat forepaw elicits robust increases in cerebral blow flow (CBF); CBV that are associated with corresponding increases in local glucose metabolism. This vascular response has been extensively used to map brain activity in cerebral cortex for brain functional studies, for example by using fMRI and diffusive optical tomography (DOT).[14–16] The fluorescence technique used can track intracellular calcium ($[Ca^{2+}]_i$) changes which are directly associated with neuronal activity, so we conducted the simultaneous measurements of CBV, S_tO_2 and $[Ca^{2+}]_i$-fluorescence to examine the feasibilities of our ODF probe to temporally dissect the events that gave rise to fMRI BOLD signals in terms of both calcium ion fluxes involved in neuronal activity and the resulting hemodynamic changes. For comparison, other experiments, including local-field potential (LFP) measurement and fMRI, were also performed in parallel in the somatosensory cortex of the additional rats.

Forepaw electrical stimulation was performed using two needle electrodes, subcutaneously in the right forepaw with one in the space between digits

two and three, and the other between digits four and five.[14] The stimulus was generated by a current source (Isolated Pulse Stimulator 2100, A-M Systems). Figure 1(c) shows the stimulus paradigm. The stimulus frequency was set to 3 Hz with 2–3 mA currents. Stimulus durations were 10 s and 30 s for LFP and CBV measurements, respectively.

2.3.5. *Acquisition of ODF, LPF, (fMRI)BOLD and data analysis*

For detecting CBV, S_tO_2, and $[Ca^{2+}]_i$-fluorescence from the cortex of the rat, the optical fiber tip was placed in contact with the cortical surface as shown in Fig. 1(a). The interface between the fiber optical tip and the brain was filled with transparent gel (Surgical Lubricant Sterile Bacteriostatic; NY) to reduce the mismatch in refractive index between fiber, air, and brain tissue, thus minimizing the specular reflection from the surface of the brain. All CBV, S_tO_2 and $[Ca^{2+}]_i$ changes were expressed as a percentage of the baseline ± SEM.

For LFP recording, a tungsten electrode (0.5 MΩ, $\phi = 0.127$ mm, A-M Systems Inc.) was inserted 0.6 mm deep into the layer III–VI of the forepaw somatosensory cortex (4 mm left from Bregma), using a three-dimensional (3D) micromanipulator (KITE-R, WPI Inc.). It was then connected to the positive socket of the head-stage pre-amplifier (1×, A-M Systems Inc.). A half-cell pellet electrode was fixed beneath the scalp and connected to the ground of the pre-amplifier. The head-stage output was fed to the main amplifier (DAM 80, WPI Inc.). The amplification was set to $10^3\times$, and the low and high cutoff frequencies were set at 0.3 KHz and 3 KHz. The whole animal fixation and the main amplifier were placed in a Faraday cage on an optic table to shield electromagnetic interference. The stereotaxic frame, manipulator, optic table, Faraday cage, and the ground outlet of the head-stage were all grounded at a single point. The output of the main amplifier was converted to digital signal by a DAQ module (1401-Plus, CED Inc.) at a rate of 20 KHz together with the TTL stimulus marker from the stimulator, and the data were stored in a PC console installed with the DAQ software (Spike2, CED Inc.).

Statistical analysis for ODF and LFP measurements was performed by using Student's t-test, and $p < 0.05$ was considered significant.

All MRI imaging was performed on a superconducting 9.4T/210 horizontal bore magnet (Magnex) controlled by an ADVANCE console (Bruker) using a 30-mm diameter surface radiofrequency coil secured above the head of the rat. After positioning and insertion of the needle electrode, the anesthesia was switched from isoflurane to α-chloralose. The procedure of fMRI has been described previously.[26] Briefly, a single-shot echo-planar sequence was used with the following parameters: TR = 1500, TE = 30 ms, FOV = 2.56×2.56 cm^2, 64×64 matrix with in-plane resolution of 400 μm; eight axial 1.4-mm–thick slices were spaced 0.15 mm apart. Each scan was acquired in three seconds. To more accurately identify the anatomical location of the functional activation maps, higher-resolution T2-weighted spin-echo images were acquired with identical spatial geometry using a RARE pulse-sequence. The fMRI scan paradigm consisted of 13 scans acquired during rest, 3 scans during stimulation and a post-stimulation rest period of 20 scans. The total acquisition time of each stimulation cycle was about ∼1.8 min.

The fMRI images were analyzed using Stimulate (CMRR, Univ. of MN). After a background masking, the intensity time curse of each pixel during the scan was cross-correlated with a boxcar template according to the known stimulation profile. We used a correlation coefficient threshold of $r \geq 0.3$ which corresponds to a p value of 0.01 to calculate the activation maps and detect the area with a statistically significant BOLD signal.[26]

3. Results

3.1. *$Rhod_2$ distribution in biological phantom and brain*

Figure 2(a) shows a 3D distribution of $Rhod_2$ as a function of the distances from the $Rhod_2$ injection center. It indicates that $Rhod_2$ was distributed equally in all directions into a wide perimeter and the 50% value of the maximal amplitude was approximately 4 mm away from the injection center. Figure 2(b) shows the comparison of $Rhod_2$ fluorescence intensities as a function of distance from the injection center obtained by using different microinjection rates. The experimental results indicated that a low injection rate (e.g., 0.1 μl/min) produced a homogeneous dye distribution within a wide perimeter (∼6 mm). However, the intensity of the fluorescence emission is extremely low and might not be detectable *in vivo* due to absorption of brain tissue with the hemoglobin. Increasing

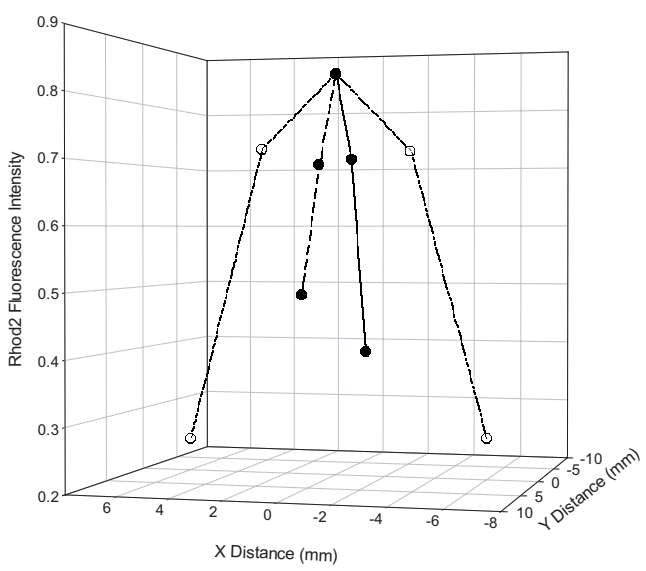

(a)

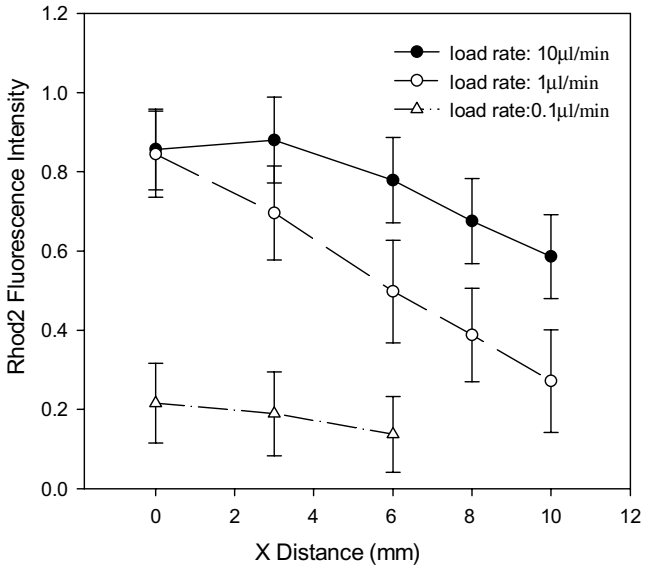

(b)

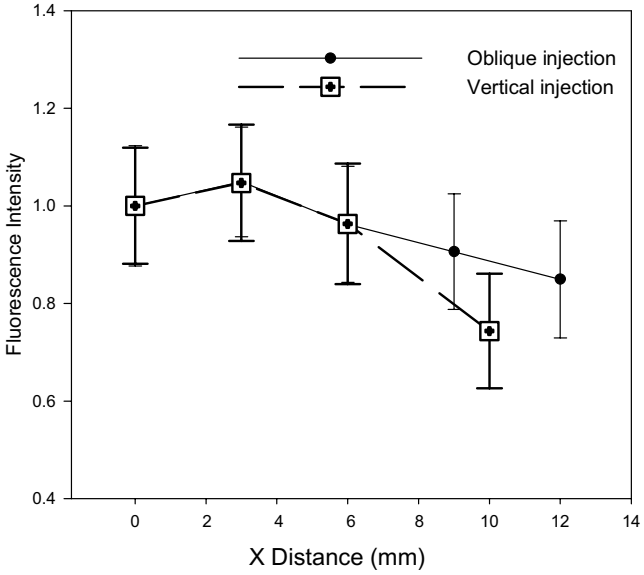

(c)

Fig. 2. Distribution of Ca-indicator, $Rhod_2$, within tissue phantoms: (a) in three dimensions, (b) within the different loading rates, and (c) with an oblique or vertical injection method.

injection rate to 1 μl/min resulted in a significant increase in the $Rhod_2$-Ca^{2+} fluorescence, as well as the diffusion distance. However, the dye concentration was remarkably attenuated as a function of the distribution distance. While the injection rate was increased to 10 μl/min, the $Rhod_2$ concentration gradient was decreased, therefore appearing like a homogeneous fluorescence emission, specifically ~ 3 mm in radius surrounding the injection center as shown in Fig. 2(b) (solid line). Figure 2(c) shows a comparison of fluorescence distribution within the phantoms between the vertical and oblique injection methods. It indicates that the oblique injection provided a better homogeneous distribution of dye over a wide region (i.e., the curve is flatter) than that obtained from vertical method. These experimental results from the phantom studies demonstrate that (1) $Rhod_2$ was distributed within a perimeter around the injection tip, and the 50% value of the maximal intensity was ~ 4 mm away

from the injection center (Fig. 2(a)) at a given flow rate; (2) the infusion rate impacted the intensity of $Rhod_2$-Ca^{2+} fluorescence emission, i.e., the higher the infusion rate, the more loading of $Rhod_2$ and the better the signal-to-noise ratio; and (3) the oblique injection (i.e., microinjection with an angle of $\sim$30–45°) can be used to improve the homogeneous distribution of $Rhod_2$ locally in a certain layer of the brain.

On the basis of these phantom studies, we performed a microinjection protocol to load $Rhod_2$ into a rat brain *in vivo* to label intracellular calcium of the brain cells. We applied the oblique injection configuration with the injection rate of 3 μl/min to optimize the $Rhod_2$(AM) distributing into cortical area of the brain according to the above phantom studies. However, the concentration of $Rhod_2$(AM) for the brain was 10-fold higher than that used in the phantom (i.e., 100 μM vs 10 μM) due to the absorption of hemoglobin within the brain. Figure 3 shows the typical $Rhod_2$ fluorescence micrographs (10×) as a function of the depth from the cortical surface of the rat brain. The little hole shown in the middle of Figs. 3(B) and 3(C) was the track of the microinjector which delivered $Rhod_2$(AM) into the brain. The $[Ca^{2+}]_i$ fluorescence labeled by $Rhod_2$(AM) can be visualized (white spots in Fig. 3) within $\sim$1.0–1.5 mm radius around the injection track (Fig. 3(B)). The higher magnification (i.e., 40×) of the same brain section could clearly show the fluorescence uptake by cells (data not shown), thus indicating the intracellular localization of the $Rhod_2$-Ca binding.

3.2. *Evaluation of tissue damage of brain due to $Rhod_2$ loading*

Figure 4(A) is a top view of the brain sectioned for redox scan in which the white box indicates the scanned region of $1.024 \times 1.024\,cm^2$. The fluorescence images are presented in Fig. 4(B)–(D). The fluorescence of $Rhod_2$-Ca^{2+} was measured simultaneously with NADH and flavoproteins Fp to present the metabolic state of the frozen brain. The ratio between the two signals of NADH and Fp measured yielded the corrected redox state independent of changes in mitochondria concentration or hemoglobin level in the tissue studied.[13] Figure 4(B) shows the tissue volume of $\sim 2^3\,mm^3$ labeled by $Rhod_2$. NADH and Fp images are shown in Figs. 4(C) and 4(D). The homogeneity of the distribution of the redox states between left side of brain ($Rhod_2$ injection side) and right side of the brain (vehicle side) suggests that there was no significant $Rhod_2$-induced damage in the brain. Specifically, there were no significant changes in NADH and Fp in the location of $Rhod_2$ presence, except directly in the needle track.

Figures 4(E) to 4(H) show a series of diffusion-weighted MR images acquired *in vivo* of the rat 1.5–2 h following the $Rhod_2$ microinjection. The $Rhod_2$ injection site was visible in the right hemisphere as a bright area surrounded by a slightly darker band. However, the apparent diffusion coefficient (ADC) value was within normal range ($\sim 0.8 \times 10^{-5}\,mm^2/s$) $>200\,\mu m$ from the needle track, thus further confirming that there was no

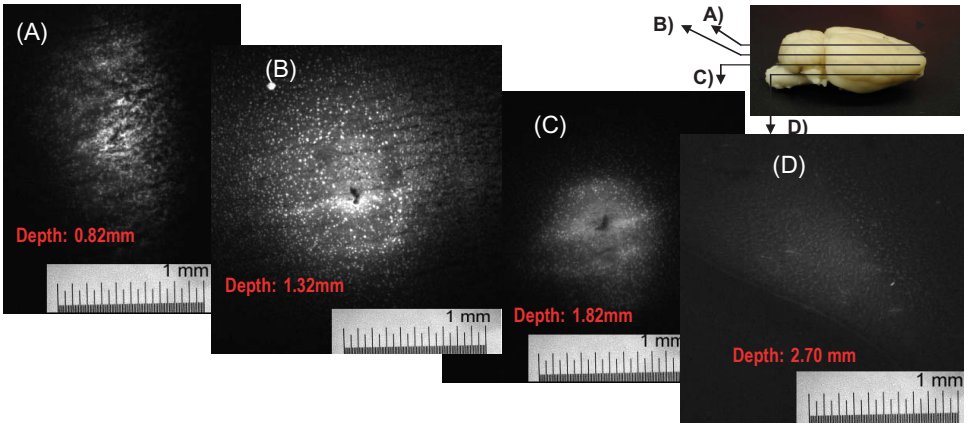

Fig. 3. Ca-dependent fluorescence micrographs labeled by using $Rhod_2$(AM) obtained from different depths of the brain, thus showing the $Rhod_2$ distribution as a function of depth within the brain. The white spots show the fluorescence uptake of the cell and indicate the intracellular localization of $Rhod_2$-Ca binding.

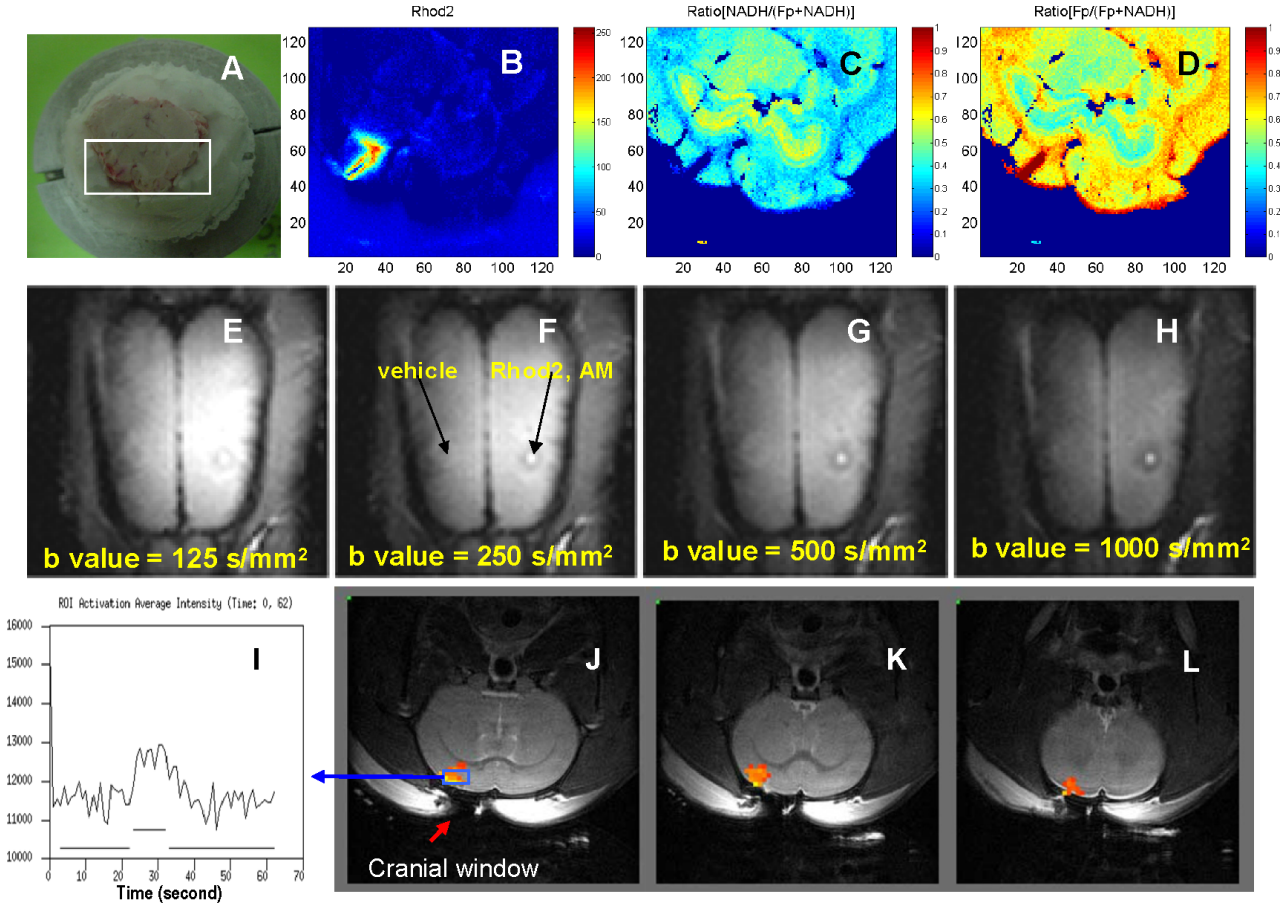

Fig. 4. Fluorescence images (top row) of *ex vivo* freeze-trapped brain and MRI (middle and bottom rows) of *in vivo* brain. (A) top view of the brain sample, (B) $Rhod_2$-Ca fluorescence emission, (C) NADH fluorescence, and (D) Flavoprotein Fp. (E)–(H) Diffusion-weighted MRI with various b values. (J)–(L) Anatomical image of the rat brain with superposing BOLD activation maps in response to forepaw stimulation. (I) The time course of the BOLD changes in ROI (blue box in (J)) in response to the stimulation. These studies indicated that there was no significant damage of brain tissue induced by craniotomy and $Rhod_2$ loading.

significant tissue ischemia/damage occurred due to $Rhod_2$ loading to affect the brain function, as ischemia would be present only if the ADC is less than $0.3–0.4 \times 10^{-5}\,mm^2/s$.[17,18]

Figures 4(J) to 4(L) show the anatomical imaging of the rat brain, and the BOLD responses to the right forepaw stimulation were superimposed on these images. The craniotomy is clearly visualized in the active side of the brain, thus suggesting the minimal effect of the invasive processes on the brain functions. Figure 4(I) is the time-course of the region of interest placed on the center of the active area of the BOLD map in Fig. 4(J), which indicates the BOLD increase as a function of time in response to the 10-second-stimulation of the forepaw. These results indicate that the mini-invasive processes used in our studies (i.e., creating a small craniotomy above the cortical surface and microinjecting $Rhod_2$(AM) into the brain) induce a minor local tissue damage, but do not affect the brain functional changes globally.

3.3. *LFP, CBV, S_tO_2 and $[Ca^{2+}]_i$ responses of brain to the electrical forepaw stimulation*

Figure 5(a) shows the time window for the stimulation period (i.e., 10 s) and the corresponding train of local field potentials (LFPs). It shows that 3-Hz stimulus pulses evoked 30 single LFP pulses during the stimulation period. Figure 5(b) is an example of the LFPs at high magnification, which indicates that a negative sharp peak was reached by 10–20 ms in response to the stimulus. It was followed by an overshoot within the LFP response and then it recovered to the baseline. Figure 5(c) shows the mean LFP peaks as a function of the time during the stimulation period in response to the different

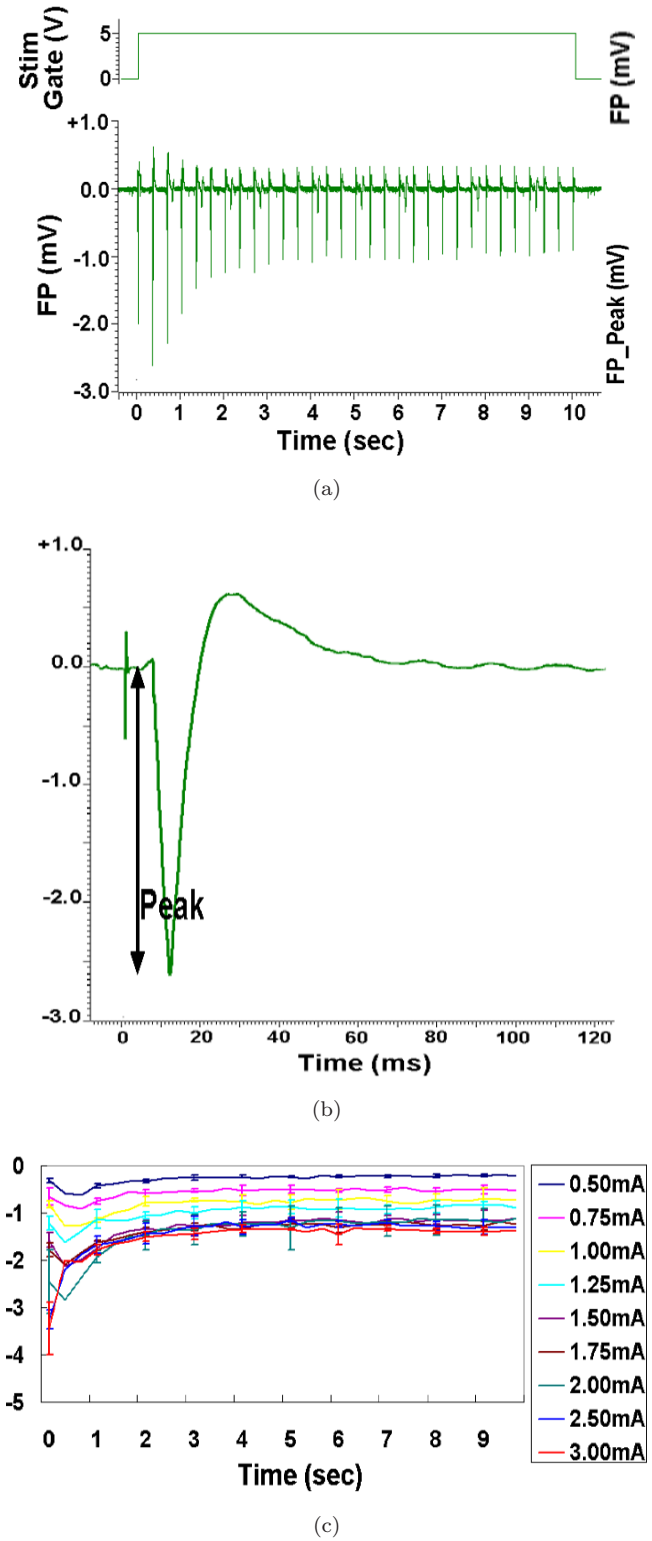

Fig. 5. Local field potential (LFP) recording of the cortex of the brain in response to electrical forepaw stimulations of 3 Hz with 10 s duration. (a) A snapshot of LFP: the upper trace is the time window for the stimulation period; the bottom is the corresponding train of LFPs during the stimulation. (b) One of the LFPs at a high magnification. (c) The peak amplitudes of the LFPs as a function of time in response to the different current intensities from 0.5 mA to 3 mA.

stimulus currents between 0.5 mA to 3 mA. As can be seen, the stimulus current over 2 mA evoked the largest LFP peak (~ -3.5 mV) at a shortest time ($<$ 20 ms), and then the LPF converged to the steady amplitude (~ 1.8 mV) within one second and stayed for the rest of the stimulation period. Based on these findings, we chose the stimulus paradigm of 3 Hz and 3 mA for the fMRI and optical experiments in order to obtain a maximal vascular and neuronal responses of the brain, but avoid the progressive attenuation within the stimulation duration.[14]

Figure 6 shows the changes in CBV, S_tO_2 and $[Ca^{2+}]_i$ fluorescence of the somatosensory response to the forepaw stimulation. The stimulation profile

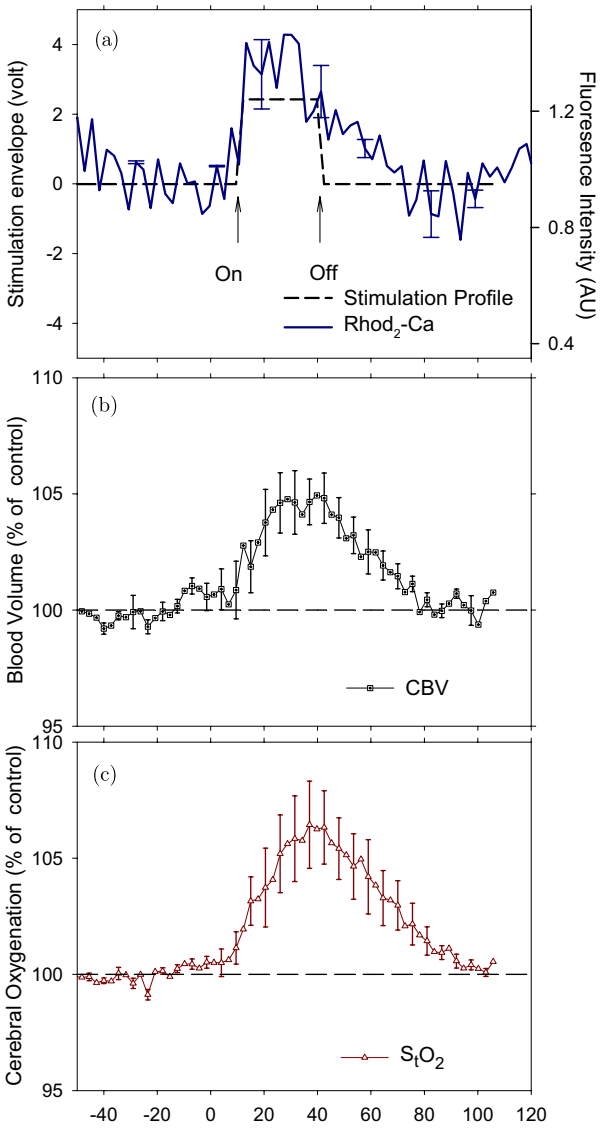

Fig. 6. Changes in $[Ca^{2+}]_i$ fluorescence of (a) $Rhod_2$, (b) cerebral blood volume, and (c) oxygenation obtained from the living rat brain in response to electronic forepaw stimulation (3 Hz, 3 mA).

is superimposed on the time-course of $[Ca^{2+}]_i$ fluorescence as shown in Fig. 6(a). CBV and S_tO_2 changes induced by forepaw stimulation are shown in Figs. 6(b) and 6(c), respectively. As can been seen, the forepaw stimulation induced $\sim$40–50% ($p < 0.02$) increase in $[Ca^{2+}]_i$ fluorescence. Concurrent increases of $\sim$3–6% ($p < 0.005$) in CBV and S_tO_2 were also observed as shown in Figs. 6(b) and 6(c), respectively. These results demonstrate the proof-on-concept that our ODF probe can be used to separately distinguish the multi-parameters and track changes of $[Ca^{2+}]_i$, CBV, and S_tO_2 in the live brain during functional activation.

4. Discussion and Conclusion

We have developed a prototype catheter-based optical probe (i.e., ODF probe) capable of simultaneous measurements of optical diffusion and the fluorescence from the surface of animal brain. This probe can detect rapid changes in cerebral blood volume (CBV), and tissue oxygenation (S_tO_2) with its optical diffusive-photon detection capability. Its fluorescence detection capability allows it to detect the simultaneous changes in intracellular calcium ($[Ca^{2+}]_i$) binding to the calcium indicator $Rhod_2$. In spite of our previous success in implementing the $Rhod_2$-Ca^{2+} fluorescence technique in studies of the whole perfused heart,[20,21] it was clearly more challenging to integrate the detection of these three parameters into one measurement. For instance, to minimize effects of hemoglobin oxygenation changes on the $Rhod_2$ excitation and emission, we selected a pair of isobestic wavelengths for excitation (e.g., 548 nm) and fluorescence emission (e.g., 589 nm). Also, the ratio of $Rhod_2$ fluorescence at 589 nm over the re-emitted excitation at 548 nm was used to eliminate the influence of the absorption and scattering changes within the tissue on the $[Ca^{2+}]_i$ fluorescence signal. To detect changes in CBV and S_tO_2, we measured the diffusive reflectance from the brain at the additional two wavelengths of 555 nm and 572 nm, which coincided with the absorption band of oxy- and deoxy-hemoglobin, and changed with the same amplitude but in opposite directions corresponding to the hemoglobin oxygenation changes. This approach was pioneered by Chance *et al.*,[7,22] and theoretically extended and experimentally validated continually.[8,20,23–25]

To validate this technique for physiological and pharmacological applications, various animal studies have been conducted. Our previous studies on a transient stroke demonstrated that the reversible forebrain ischemia induced the simultaneous changes of CBV, S_tO_2 and $[Ca^{2+}]_i$ that can be detected by the ODF probe.[9] The increase of $[Ca^{2+}]_i$ fluorescence induced by the ischemic insult was inhibited by L-type calcium channel blocker (nimodipine), thus suggesting that the $[Ca^{2+}]_i$ fluorescence signal was derived from the intracellular compartment. In other words, the ischemic-induced increase of $Rhod_2$ fluorescence reflected the $[Ca^{2+}]_i$ increase, not due to $Rhod_2$ leaking out to the extracellular space. In addition, the ODF probe was also used to track the brain responses to the stimulants such as cocaine,[10] although the pharmacologically-induced signal changes within the brain were much smaller (i.e., $\sim$3–4% changes in CBV, S_tO_2, $p < 0.05$) than those (i.e., $\sim$40–50% changes in CBV, S_tO_2, $p < 0.001$) induced by a robust physiological challenge such as an ischemic insult. These results demonstrate the feasibility of the optical technique presented here for physiological and pharmacological phenotyping.

To characterize the hemodynamic coupling with the neuronal activation of the brain, the electrical forepaw stimulation animal model was used, and the somatosensory cortical responses were recorded using fMRI (Fig. 4), LFP (Fig. 5) and ODF probes (Fig. 6). The simultaneous changes in CBV, S_tO_2 and $[Ca^{2+}]_i$ fluorescence were detected from the somatosensory cortex of the rat brains, and the responses were comparable with the fMRI BOLD signals but with a higher temporal resolution ($\sim$ms). In addition, the ODF probe can be used to separately distinguish the multi-parameters at real time. The fact of tracking $[Ca^{2+}]_i$ fluorescence along with CBV and S_tO_2 changes in the living brain during the brain activation provided a new modality for functional brain studies using optical imaging.[14,16]

In summary, we presented an ODF probe to detect the fluorescence emission and diffuse reflectance from the brain surface based on the concept of time sharing at multiple wavelengths. This approach may open new opportunities to study the function of normal or diseased brains to understand the cerebral pathological processes such as a drug-driven cell injury or brain functional changes.

Acknowledgments

This work was supported in part by NIH Grants K25-DA021200, Laboratory Directed Research

Development (LDRD) Grant (04-066) of Brookhaven National Laboratory, and by Department of Energy Office of Science and Biological Research.

References

1. Breiter, H. C., Gollub, R. L., Weisskoff, R. M., Kennedy, D. N., Makris, N., Berke, J. D., Goodman, J. M., Kantor, H. L., Gastfriend, D. R., Riorden, J. P., Mathew, R. T., Rosen, B. R. and Hyman, S. E., "Acute effects of cocaine on human brain activity and emotion," *Neuron* **19**, 591–611 (1997).
2. Rissman, J., Gazzaley and D'Esposito, M., "Measuring functional connectivity during distinct stages of a cognitive task," *NeuroImage* **23**, 752–763 (2004).
3. Lee, J. H., Telang, F. W., Spring, C. S. and Volkow, N. D., "Abnormal brain activation to visual stimulation in cocaine abusers," *Life Sciences* **73**, 1953–1961 (2003).
4. Gur, R. C., Ragland, J. D., Reivich, M., Greenberg, J. H., Alavi, A. and Gur, R. E., "Regional differences in the coupling between resting cerebral blood flow and metabolism may indicate action preparedness as a default state," *Cerebral Cortex* **19**, 375–382 (2009).
5. Dale, A. M., Liu, A. K., Fischl, B. R., Buckner, R. L., Belliveau, J. W., Lewine, J. D. and Halgren, E., "Dynamic statistical parametric mapping: Combinig fMRI and MEG for high-resolution imaging of cortical activity," *Neuron* **26**, 55–67 (2000).
6. London, E. D., Bonson, K. R., Ernst, M. and Grant, S., "Brain imaging studies of cocaine abuse: Implications for medication development," *Critical Reviews in Neurobiology* **13**(3), 227–242 (1999).
7. Chance, B., Cohen, P., Jobsis, F. and Schoener, B., "Intracellular oxidation-reduction state *in vivo*," *Science* **137**, 499–508 (1962).
8. Baos, D. A., Franceschini, M. A., Dunn, A. K. and Strangman, G., "Noninvasive imaging of cerebral activation with diffuse optical tomography," Chapter 8, in *In Vivo Optical Imaging of Brain Function*, ed. Frostig, R. D. (CRC Press, 2002).
9. Du, C., Koretsky, A. P., Izrailtyan, I. and Benveniste, H., "Simultaneous detection of blood volume, oxygenation, and intracellular calcium changes during cerebral ischemia and reperfusion *in vivo* using diffuse reflectance and fluorescence," *J. Cereb. Blood Flow Metab.* **25**, 1078–1092 (2005).
10. Du, C., Yu, M., Volkow, N. D., Koretsky, A. P., Fowler, J. S. and Benveniste, H., "Cocaine increases the intracellular calcium concentration in brain independently of its cerebralovascular effects," *J. Neuroscience* **26**(45), 11522–11531 (2006).
11. Kudo, Y., Akita, K., Nakamura, T., Ogura, A., Makino, T., Tamagawa, A., Ozaki, K. and Miyakawa, A., "A single optical fiber fluorometric device for measurement of intracellular Ca^{2+} concentration: Its application to hippocampal neurons *in vitro* and *in vivo*," *Neuroscience* **50**, 619–625 (1992).
12. Takakashi, M. P., Sugiyama, M. and Tsumoto, T., "Contribution of NMDA receptors to tetanus-induced increase in postsynaptic Ca in visual cortex of young rats," *Neurosci. Res.* **17**, 229–239 (1993).
13. Chance, B., Schoener, B., Oshino, R., Itshak, F. and Nakase, Y., "Oxidation-reduced ratio studies in freeze-trapped samples," *J. Biol. Chem.* **254**, 4764–4771 (1979).
14. Silva, A. C., Lee, S. P., Yang, G., Iadecola, C. and Kim, S. G., "Simultaneous blood oxygenation level-dependent and cerebral blood flow functional magnetic resonance imaging during forepaw stimulation in the rat," *J. Cereb. Blood Flow Metab.* **19**(8), 871–879 (1999).
15. Masamoto, K., Kim, T., Fukuda, M., Wang, P. and Kim, S. G., "Relationship between neural, vascular, and BOLD signals in isoflurane-anesthetized rat somatosensory cortex," *Cereb. Cortex* **17**(4), 942–950 (2007).
16. Dunn, A. K., Devor, A., Dale, A. M. and Boas, D. A., "Spatial extent of oxygen metabolism and hemodynamic changes during functional activation of the rat somatosensory cortex," *NeuroImage* **27**, 279–290 (2005).
17. Benveniste, H., Hedlund, L. W. and Johnson, G. A., "Mechanism of detection of acute cerebral ischemia in rats by diffusion-weighted magnetic resonance microscopy," *Stroke* **23**(5), 746–754 (1992).
18. Liu, K. F., Li, F., Tatlisumak, T., Garcia, J. H., Sotak, C. H., Fisher, M. and Fenstermacher, J. D., "Regional variations in the apparent diffusion coefficient and the intracellular distribution of water in rat brain during acute focal ischemia," *Stroke* **32**(8), 1897–1905 (2001).
19. Benveniste, H., Jørgensen, M. B., Diemer, N. H. and Hansen, A. J., "Calcium accumulation by glutamate receptor activation is involved in hippocampal cell damage after ischemia," *Acta. Neurol. Scand.* **78**(6), 529–536 (1988).
20. Du, C., MacGowan, G. A., Farkas, D. L. and Koretsky, A. P., "Calcium measurements in perfused mouse heart: Quantitating fluorescence and absorbance of Rhod2 by application of photon migration theory," *Biophys. J.* **80**(1), 549–561 (2001).
21. MacGowan, G. A., Du, C., Glonty, V., Suhan, J. P., Koretsky, A. P. and Farkas, D. L., "Rhod2-based measurements of intracellular calcium in the perfused mouse heart: Cellular and subcellular localization and response to positive inotropy," *J. Biomed. Opt.* **6**(1), 23–30 (2001).
22. Chance, B., Nioka, S., Sadi, S. and Li, C., "Oxygenation and blood concentration changes in human subject prefrontal activation by anagram solutions," *Adv. Exp. Med. Biol.* **510**, 397–401 (2003).

23. Sevick, E. M., Chance, B., Leigh, J., Nioka, S. and Maris, M., "Quantitation of time- and frequency-resolved optical spectra for the determination of tissue oxygenation," *Anal. Biochem.* **195**(2), 330–351 (1991).
24. Nioka, S., Luo, Q. and Chance, B., "Human brain functional imaging with reflectance CWS," *Adv. Exp. Med. Bio.* **428**, 237–242 (1997).
25. Culver, J. P., Durduran, T., Furuya, D., Cheung, C., Greenberg, J. H. and Yodh, A. G., "Diffuse optical tomography of cerebral blood flow, oxygenation, and metabolism in rat during focal ischemia," *J. Cereb. Blood Flow Metab.* **23**(8), 911–924 (2003).
26. Luo, Z. C., Yu, M., Smith, S. D., Kritzer, M., Du, C., Ma, Y., Volkow, N. D., Glass, P. S. and Benveniste, H., "The effect of intravenous lidocaine on brain activation during non-noxious and acute noxious stimulation of the forepaw: A functional magnetic resonance imaging study in the rat," *Anesthesia & Analgesia* **108**(1), 334–344 (2009).